THE JOURNAL OF PHYSICAL CHEMISTRY B

ARTICLE

pubs.acs.org/JPCB

Resonance Raman Spectroscopic and Theoretical Investigation of the Excited State Proton Transfer Reaction Dynamics of 2-Thiopyridone

Rui Du,[†] Chong Liu,[†] Yanying Zhao,[†] Ke-Mei Pei,[†] Hui-Gang Wang,[†] Xuming Zheng,[*,†,‡] Mingde Li,[§] Jia-Dan Xue,[§] and David Lee Phillips[*,§]

[†]Department of Chemistry, Zhejiang Sci-Tech University, Hangzhou 310018, China

[‡]State Key Laboratory of Advanced Textiles Materials and Manufacture Technology, MOE, Zhejiang Sci-Tech University, Hangzhou 310018, China

[§]Department of Chemistry, The University of Hong Kong, Pokfulam Road, Hong Kong SAR, China

ABSTRACT: The resonance Raman spectra were obtained for both 2-thiopyridone (2TP) and its proton-transfer tautomer 2-mercaptopyridine (2MP) in water solution. Density functional theory (DFT) calculations were carried out to help elucidate their ultraviolet electronic transitions and vibrational assignments of the resonance Raman spectra associated with their B-band absorptions. The nanosecond time-resolved resonance Raman spectroscopic experiment was carried out to further confirm the assignment that the transient species was the ground state 2MP. The different short-time structural dynamics were examined for both 2TP and 2MP in terms of their resonance Raman intensity patterns. The transition barriers between 2TP and 2MP for S_0, T_1, and S_1 states are determined by using (U)B3LYP-TD and CASSCF level of theory computations, respectively. The excited state proton transfer (ESPT) reaction mechanism is proposed and briefly discussed.

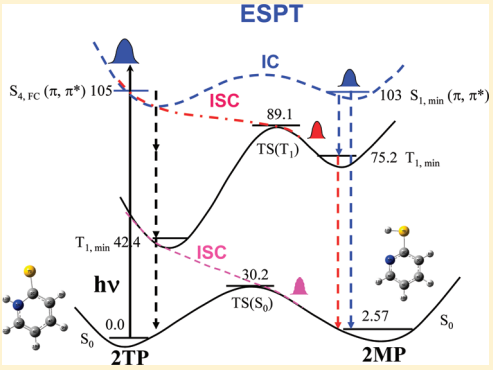

1. INTRODUCTION

The enol−keto tautomerization reaction between 2-hydroxypyridine (2HP) and 2-pyridone (2PY) has been extensively studied experimentally[1−11] and theoretically[12−25] because of its importance in organic chemistry and biochemistry.[26,27] In the gas phase 2HP and 2PY are nearly equal in energy with the enol form being more stable than keto form by 3.5 KJ/mol.[7,8,24] However, the ground state proton transfer tautomerization reaction is practically prohibited due to a very large transition barrier (34−38 kcal/mol) between 2HP and 2PY.[13,16,18] Increasing the number of OH groups attached to aromatic, heterocyclic rings and the number of N atoms in the ring significantly shifts the tautomeric equilibrium toward the keto form, as in going from 2-OH pyridine to 4-OH pyrimidine and/or to uracil.[9] The excited state proton transfer (ESPT) reaction between 2HP and 2PY were studied by using spectroscopic and theoretical methods in the gas phase and the condensed phase,[1,7,12,14,15,17,18,25] but no clear experimental evidence has been obtained so far for ESPT reaction of 2HP.[1,11]

2MP and 2TP are respectively the S-substituted derivatives of 2HP and 2PY. The ground state thio−thione tautomerization reaction between 2TP and 2MP has been studied extensively in condense phases (Scheme 1) due to its biological importance.[7,28−40] Thiol tautomer or 2MP (structure II) exists dominantly in the diluted solution of nonpolar solvent and in the vapor phase, while thione tautomer, or 2TP (structure I), dominates the equilibrium in the neutral water solution. The experimental investigations from the ultraviolet spectroscopy[29] and free jet microwave (MW) spectroscopy as well as core level photoemission spectroscopy[30] reveal that 2MP is the major protomeric isomer in the vapor. However, crystallographic studies of several nitrogen-containing heterocyclic thiones show that the 2TP appears predominantly in the solid state,[41] although the weak intensity IR band in the region 2500−2600 cm^{-1} were assigned to the −SH stretching mode.[42,43] Abdulla and El-Bermani[44] studied the IR spectra of 2MP in solid, liquid, and vapor phases and its deuterated form. The results were interpreted in terms of the equilibrium mixture of two monomeric

Scheme 1. Structures and Atom Labelings of 2TP and 2MP

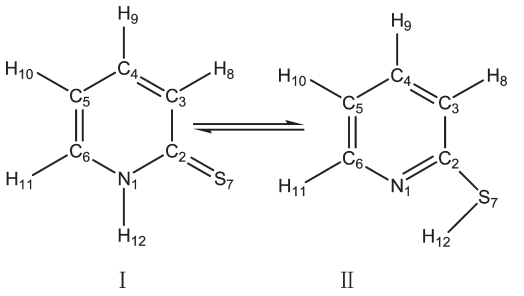

Received: November 11, 2010
Revised: May 21, 2011
Published: May 26, 2011

tautomers and three cyclic dimers with the monomers being the predominant species in the vapor phase.

The photomeric tautomerization reaction between 2TP and 2MP has not been reported. In this paper, we present for the first time the transient resonance Raman and the nanosecond time-resolved resonance Raman spectra of 2MP in water solution formed from B-band photoexcitation of 2TP. We present results from density functional theory (DFT) computations for both the vibrational spectra and UV absorption spectra of 2MP and 2TP and compare these to our present experimental results and previously reported IR spectra.[44] The ESPT reaction mechanism was proposed with the aid of CASSCF and time-dependent density functional theory (TD-DFT) computations made for both 2MP and 2TP. Our results indicate that the ESPT reaction of 2TP in water solution leads to the formation of the ground state 2MP transient species, which constitutes an important excited state decay channel for 2TP upon 266 nm excitation.

2. EXPERIMENTS AND COMPUTATIONAL METHODS

The Fourier transform (FT) Raman and FT-IR spectra were obtained using a Thermo Nicolet FT-Raman 960 spectrometer and a Perkin-Elmer 1 FT-IR spectrometer with 2 cm^{-1} resolution. The UV absorption spectrum was measured in water solution using ultraviolet/visible spectrometer. The experimental apparatus used to acquire the B-band resonance Raman spectra of 2TP and the transient resonance Raman spectra of 2MP have been described previously[45−49] so only a short description will be provided here. The 266 nm excitation wavelength for the resonance Raman experiments was supplied by the fourth harmonics of a nanosecond Nd:YAG laser. High- and lower-power spectra were obtained and the transient resonance Raman spectra were derived by subtracting the lower-power spectrum from the high-power spectrum. The intensity dependent Raman bands of the lower-power spectra displayed a roughly quadratic dependent on power in a limited weak power range, and this means that the 266 nm resonance Raman spectrum of the parent 2TP molecule (see Figures 3, 4B, and 7) is due to a one-photon process. When the higher power is used to obtain the high pulse energy difference spectrum (that is, the transient resonance Raman spectra of the photoproducts), the laser power dependence of the Raman intensity of the parent 2TP molecule relative to that of the water solvent displays the occurrence of the bulk photoalternation in higher laser power, and this indicates that the high pulse energy difference spectrum (Figures 4C, 5d, and 6) is formed from a two-photon process. The solution phase samples used concentrations of approximately ∼6.0 × 10^{-3} mol·L^{-1} 2TP (99% purity) in water and in spectroscopic grade acetonitrile (99.5+ % purity) solvent. The excitation laser beam used a ∼100 μJ pulse energy loosely focused to a 0.5−1.0 mm diameter spot size onto a flowing liquid stream of sample to excite the sample. Power-dependent experiments were done using ∼100 μJ pulse energy focused on a beam diameter of ∼1.0 mm for lower energy spectra and ∼260 μJ pulse energy focused on a beam diameter of ∼0.5 mm for higher energy spectra, respectively. A backscattering geometry was employed to excite a flowing liquid jet of sample and collect the Raman scattered light with reflective optics that imaged the light through a polarizer and entrance slit of a 0.5 m spectrograph. The grating of the spectrograph dispersed the Raman scattering light onto a liquid nitrogen-cooled charge coupled device (CCD) detector. The Raman signal was collected for about 90−120 s before being read out to an interfaced PC computer, and 30−40 of these readouts were added together to get the resonance Raman spectrum. The Raman shifts of the resonance Raman spectra were calibrated with the known vibrational frequencies of the cyclohexane solvent Raman bands, and the solvent Raman bands were then subtracted from the resonance Raman spectra by utilizing an appropriately scaled solvent spectrum. Sections of the resonance Raman spectra were fit to a baseline plus a sum of Lorentzian bands to determine the integrated areas of the Raman bands of interest.

Nanosecond time-resolved resonance Raman (ns-TR^3) experimental apparatus and methods have been detailed previously[50] so only a short description will be given here. The ns-TR^3 experiments employed two Nd:YAG lasers that were electronically synchronized via a pulse delay generator to control the relative timing of their flashlamps and Q switches. The relative timing of the 266 nm pump and 266 nm probe laser pulses was monitored using a fast photodiode whose output was displayed on a 500 MHz oscilloscope. The jitter was found to be <5 ns. The laser beams were lightly focused onto a flowing liquid stream of sample using a near collinear geometry, and the Raman scattered light was acquired using a backscattering geometry. The Raman light was then imaged through a depolarizer and entrance slit of a 0.5 m spectrograph and dispersed by a grating onto a liquid nitrogen-cooled CCD detector mounted on the exit of the spectrograph. The Raman signal was accumulated for about 200−300 s by the CCD detector before being read out to an interfaced personal computer. About 10−20 of these readouts were summed to obtain a resonance Raman spectrum. Pump-only, probe-only, and pump−probe resonance Raman spectra were acquired as well as a background scan. The probe-only spectrum was subtracted from the pump−probe spectrum to remove precursor and solvent Raman bands, and then the pump-only spectrum and background scan were also subtracted to obtain the time-resolved resonance Raman spectrum. The subtraction parameter used a proper constant multiplying the probe-only or the pump-only spectrum before it was subtracted from the pump−probe resonance Raman spectrum.

The complete geometry optimization and vibrational frequency computations were done using the (U)B3LYP/6-311+G(d,p) level of theory and C_s symmetry for ground and lowest triplet state 2TP and 2MP. The vertical transition energy for $S_0 \rightarrow S_n$ were estimated at B3LYP-TD/6-311+G(d,p) levels of theory employing a self-consistent reaction field (SCRF) and polarized continuum overlapping spheres model (PCM). The minimum energies and the optimized geometric structures in S_1 state are estimated by using the CASSCF(6,8)/6-311+G(d,p) level of theory and C_1 symmetry. All of the DFT calculations were done using the *Gaussian 03* program.[51]

3. RESULTS AND DISCUSSION

3.1. Electronic Transitions of 2TP and 2MP. Figure 1 presents the UV absorption spectrum of 2TP in water solution with the wavelength for the resonance Raman experiments indicated above the spectrum and the schematic geometry structure inserted. The spectrum displays respectively two strong bands at 341.6 nm (f = 0.1145 or ε = 8.176 × 10^3 L·mol^{-1}·cm^{-1}) and 270.4 nm (f = 0.1593 or ε = 1.168 × 10^4 L·mol^{-1}·cm^{-1}) within the 200−400 nm spectrum region. Time-dependent density functional theory calculations (TD-DFT) are done to help assign the absorption spectrum, and the results are listed in Table 1.

Table 1 shows that the predicted electronic transition energies of 2TP display consistently two allowed transitions at ~345 nm (f = 0.1402) and ~278 nm (f = 0.3421). Thus two experimental strong absorption bands at ~341.6 nm (A-band) and ~270.4 nm (B-band) for 2TP are tentatively assigned to $\pi \rightarrow \pi^*$ electron transitions. It appears that the 266 nm excitation wavelength used in the resonance Raman experiments is in resonance with the B-band absorption of 2TP. TD-DFT calculations are also done for 2MP to help predict its UV absorption spectrum, and the results are listed in Table 1. Within the calculated spectral region for singlet transitions, the $\pi \rightarrow \pi^*$ electronic transitions at 270 and 240 nm for 2MP have the largest oscillator strengths (f = 0.0826 and 0.2743, respectively). It appears that the 266 nm excitation wavelength used to obtain the B-band resonance Raman spectrum of 2TP is probably in resonance with the predicted 240 nm and/or 272 nm band absorptions of 2MP.

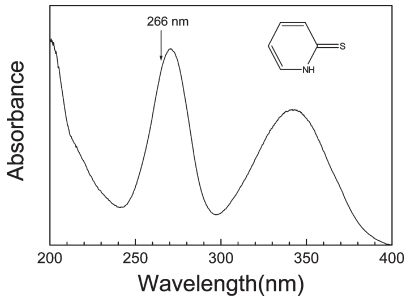

Figure 1. UV absorption spectrum of 2-thiopyridone in water solution with the geometric structure inserted.

The accuracy of the TD-DFT calculations using four different basis sets and PCM solvation model is examined for the electronic transition energies and oscillator strengths. The calculations using the 6-31+G(d), 6-311++G(d,p), and 6-311++G-(df,pd) basis sets display consistently 12 electronic transitions above 200 nm spectral region with the corresponding vertical transition energies and oscillator strengths being similar. The 6-31G(d) basis sets seem to be not large enough for consistent results. Hydrogen bonding interaction is also examined by adding respectively one or two water molecules to the C═S and/or −NH moieties of 2TP molecule, and the results display no significant changes in both the transition energies and the corresponding oscillator strengths. This indicates that the effect of hydrogen bonding interaction on the transition energies and the corresponding oscillator strengths is not significant for 2TP. Solvation interaction seems to be important for the first absorption band of the UV spectrum since its experimental oscillator strength depends largely on the polarity of solvent (f = 0.1145 for water, and f = 0.0712 for methanol) and the B3LYP-TD/6-311+G(d,p) level of theory using the PCM solvation model gives a better prediction of both electronic transition energy and the oscillator strength (345 nm, f = 0.1402) than that (373 nm, f = 0.0546) without solvation.

Figure 2 presents the molecular orbitals associated with the electronic transitions of the UV absorptions of 2TP and 2MP. To help understand the electronic structures of the excited states, we shall briefly characterize the frontier molecular orbitals as listed in Table 1. Taking 2TP as example, the highest occupied molecular orbital (HOMO) is a π-type orbital (designated as π_H) and belongs to the A′ irreducible representation. The second highest occupied MO is a nonbonding in-plane orbital (n) with most

Table 1. Singlet Electron Transition Energies and Oscillator Strengths Predicted by Using B3LYP-TD/6-311+G(d,p) Levels of Theory Employing a Self-Consistent Reaction Field (SCRF) and Polarized Continuum Overlapping Spheres Model (PCM) for 2-Thiopyridone and 2-Mercaptopyridine in Water Solution

state (Cs)	orbital	character	singlet transition energies		oscillator strengther	
			calc./nm	expt./nm	calc.	expt.
			2TP			
S_1 ($1\,^1A''$)	28→30	n→π_L^*	364		0.0002	
S_2 ($1\,^1A'$)	29→30	π_H→π_L^*	345	341.6	0.1402	0.1145
S_3 ($2\,^1A''$)	28→31	n→π_L^*	292		0.0002	
S_4 ($2\,^1A'$)	29→31	π_H→π_{L+1}^*	278	270.4	0.3421	0.1593
S_5 ($3\,^1A''$)	29→32	π_H→Ryd_1	240		0.0323	
S_6 ($3^1A'$)	28→32	n→Ryd_1	228		0.0725	
S_7 ($4^1A''$)	29→33	π_H→Ryd_2	215		0.0222	
S_8 ($4\,^1A'$)	28→33	n→Ryd_2	209		0.0235	
S_9 ($5\,^1A''$)	29→34	π_H→Ryd_3	206		0.0027	
S_{10} ($5^1A'$)	27→30	π_{H-1}→π_L^*	206		0.0311	
S_{11} ($6\,^1A'$)	28→34	n→Ryd_3	205		0.0108	
			2MP			
S_1 ($1\,^1A'$)	29→30	π_H→π_L^*	270		0.0826	
S_2 ($1\,^1A''$)	28→30	n→π_L^*	242		0.0045	
S_3 ($2\,^1A'$)	29→31	π_H→π_{L+1}^*	240		0.2743	
S_4 ($2\,^1A''$)	29→32	π_H→Ryd_1	233		0.0060	
S_5 ($3\,^1A''$)	28→31	n→π_{L+1}^*	227		0.0009	
S_6 ($4\,^1A''$)	29→33	π_H→Ryd_2	211		0.0360	
S_7 ($5\,^1A''$)	29→34	π_H→Ryd_3	200		0.0000	

dx.doi.org/10.1021/jp203185a |J. Phys. Chem. B 2011, 115, 8266–8277

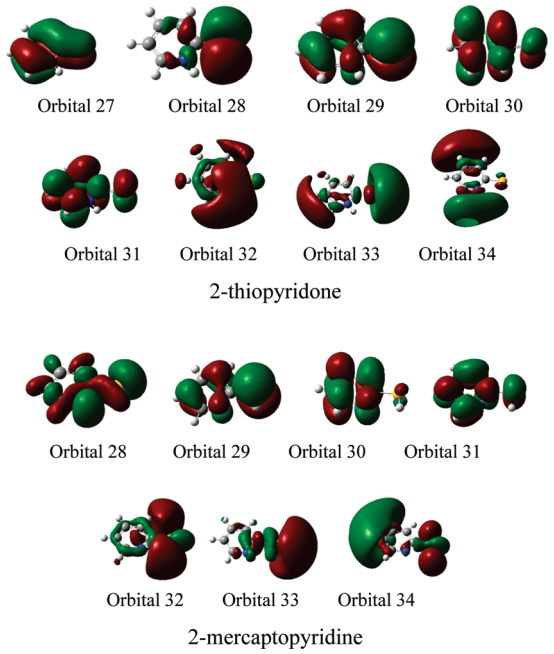

Figure 2. Molecular orbitals associated with the electronic transitions of the UV absorptions of 2-thiopyridone and 2-mercaptopyridine.

amplitude for the S lone-pair orbital. The third highest occupied MO is also a π-type orbital ($\pi_{H\text{-}1}$) in the A′ irreducible representation. The first two lowest-lying unoccupied molecular orbitals (LOMO and LOMO+1) are π_L^* and π_{L+1}^*. Three diffuse orbitals are found in energy higher than π_L^*, and they are designated as Ryd_n.[52] Ryd_1 has its major density in an area including two H atoms in the N_1-H and C_6-H bonds. The main density of Ryd_2 locates at S atom and two H atoms of the C_5-H/C_6-H bonds, while that of Ryd_3 populates in four H atoms of the $N_1-H/C_6-H/C_3-H/C_4-H$ bonds. Similar descriptions can be achieved for 2MP.

3.2. FT-Raman and Resonance Raman Spectra of 2TP. The infrared spectra of 2TP were previously studied in solid, liquid, and vapor phases.[44] The results showed that an equilibrium mixture of two monomeric tautomers and three cyclic dimers existed in three phases. Thione is the predominant form in liquid phase since the enthalpy differences between thione form (structure I) and thiol form (structure II) are estimated to be −5.20 KJ/mol based on the B3LYP/6-311+G(d,p) computation. To supplement the Raman frequencies in whole spectrum region and the information of the irreducible representations of the vibrational modes, which are proven to be useful in determining the vibrational assignments of the resonance Raman spectra, we have measured the FT-Raman spectra of 2TP and carried out the B3LYP/6-311+G(d,p) computations for both 2TP and 2MP. Figure 3 displays the FT Raman spectra of 2TP in crystalline solid state and in H_2O solvent. Table 2 lists the experimental and B3LYP/6-311+G(d,p) calculated vibrational frequencies and their tentative assignments for 2TP. We note that all vibrational modes in C_s point group are Raman and IR active. Twenty Raman bands are discerned in the region 100−1700 cm^{-1} of the solid state FT-Raman spectrum, among which 16 and 4 Raman bands are respectively assigned to A′ and A″ irreducible representations. The agreement between the calculated and the experimental vibrational frequencies is fairly good with the mean error being ±11 cm^{-1}. The solid state vibrational

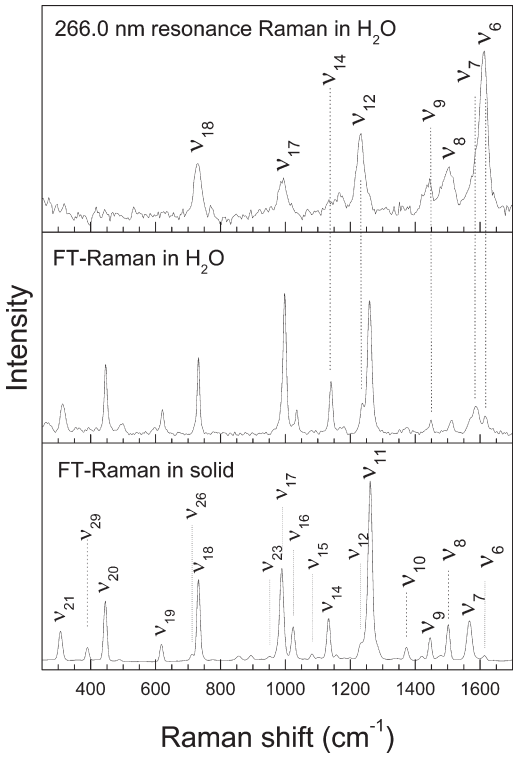

Figure 3. 266 nm resonance Raman (top) and FT-Raman spectra of 2-thiopyridone in polycrystalline solid state (bottom) and in H_2O solution (middle).

frequencies are similar to those in water solution for most of the Raman bands of 2TP. This indicates that solvation and/or hydrogen bonding interaction of water with 2TP do not affect the vibrational frequencies significantly. *Syn* and *anti* conformations of 2MP are examined, and the *syn* isomer is the global minimum and responds to the IR and Raman spectra.

The A-band (341 and 354 nm) resonance Raman spectrum of 2TP is not obtained due to very strong interference of fluorescence. The vibrational assignment for 266.0 nm (B-band) resonance Raman spectrum is achieved through direct comparison to the FT-Raman spectrum in H_2O solution, as shown in Figure 3. It appears that most of the B-band resonance Raman features can be assigned as about eight totally symmetric fundamentals: the $C_3{=}C_4/C_5{=}C_6$ stretch + ring deformation ν_6 at 1614 cm^{-1}, the $C_2C_3/C_5{=}C_6$ stretch ν_8 at 1505 cm^{-1}, the $C_3{=}C_4/N_1C_6$ stretch ν_9 at 1445 cm^{-1}, the $N_1H/C_6H/C_3H$ bend ν_{12} at 1233 cm^{-1}, the $C_2{=}S$ stretch + ring deformation ν_{17} at 994 cm^{-1}, the $C_2{=}S$ stretch + ring deformation ν_{18} at 731 cm^{-1}, the $C_3{=}C_4-C_5$ asym stretch + ring deformation ν_7 at 1565 cm^{-1}, and the C_2S stretch + $C_1H/C_2H/C_5H/C_6H$ bend ν_{14} at 1167 cm^{-1}.

3.3. Transient and Time-Resolved Resonance Raman Spectra of 2MP. Figure 4 shows the power-dependent 266.0 nm resonance Raman spectra of 2TP in water solution. The ∼80−100 μJ pulse energy is the lowest laser energy that can be used for 266.0 nm resonance Raman experiments. The results show that the resonance Raman spectrum obtained by using ∼80−100 μJ pulse energy focused on a beam diameter of ∼1.0 mm is very similar to that for ∼150 μJ pulse energy focused on a same beam diameter, and this indicates that the spectrum B in Figure 4 represents mostly the resonance Raman spectrum of the ground

dx.doi.org/10.1021/jp203185a |J. Phys. Chem. B 2011, 115, 8266–8277

Table 2. Experimental FT-IR and FT Raman Vibrational Bands and B3LYP/6-311+G(d,p) Calculated Vibrational Frequencies for the Ground State 2-Thiopyridone

	calc.			expt.					
				FT Raman		FT-IR[c]		R.Raman	
mode	*a*	*b*	scanning	in solid	in water	in solid	*c*	in H_2O	description
A′									
ν_1	3569(49/67)	3462	3502						N_1-H stretch
ν_2	3225(2/234)	3128	3166						$C_5H(s)/C_6H/C_3H/C_4H$ stretch
ν_3	3217(0.6/51)	3120	3158						$C_3H(s)/C_4H/C_5H/C_6H$ stretch
ν_4	3207(0.7/69)	3111	3148						$C_5H(s)/C_6H(s)/C_3H/C_4H$ stretch
ν_5	3177(8/114)	3082	3119						$C_4H(s)/C_3H(s)/C_5H$ stretch
ν_6	1658(83/2)	1608	1632	1614 w	1615 m	1608(s)	1618 s	1614 s	$C_3=C_4/C_5=C_6$ stretch + ring deformation
ν_7	1594(290/53)	1546	1569	1567 m	1589 m	1569(m)	1577 s		$C_3=C_4-C_5$ asym stretch + ring deformation
ν_8	1504(37/27)	1459	1481	1502 m	1514 m	1492(m)	1500 s	1505 m	$C_2C_3/C_5=C_6$ stretch
ν_9	1474(0.6/40)	1430	1452	1446 w	1448 m		1445 vs	1445 m	$C_3=C_4/N_1C_6$ stretch
ν_{10}	1386(7/34)	1344	1366	1373 w					$C_2C_3/C_5=C_6$ stretch
ν_{11}	1277(15/81)	1239	1259	1261 s	1260 s		1260 s		N_1C_2 stretch
ν_{12}	1234(5/10)	1197	1217	1230 w	1237 m	1222(m)	1236 s	1232 s	$N_1H/C_6H/C_3H$ bend
ν_{13}	1184(23/6)	1148	1168	1155 w		1164(s)			C_2S stretch + $C_1H/C_2H/C_5H/C_6H$ bend
ν_{14}	1159(199/13)	1124	1143	1131 m	1141 m				C_2S stretch + $C_1H/C_2H/C_5H/C_6H$ bend
ν_{15}	1098(15/3)	1065	1084	1081 w			1089 w		$N_1C_5=C_6$ sym stretch
ν_{16}	1030(3/13)	999	1017	1023 m	1034 m				C_4C_5 stretch
ν_{17}	993(63/7)	963	981	989 s	998 s	983(m)	992 ssh	994 m	C_2S stretch + ring deformation
ν_{18}	747(3/22)	725	740	732 s	731 s	738(m)		731 s	C_2S stretch + ring deformation
ν_{19}	627(0.5/4)	608	623	617 w	618 m				ring deformation
ν_{20}	453(10/19)	439	452	445 s	446 s		457 s		C_2S stretch + ring deformation
ν_{21}	308(1/2)	299	310	306 m	307 m		330 s		C_2S bend + ring bend
A″									
ν_{22}	1011(0.1/0.2)	981	998						$C_3H(s)/C_4H/C_5H$ wag (oop)
ν_{23}	952(0.2/2)	923	941	950 w					$C_5H(s)/C_6H/N_1H/C_3H$ wag (oop)
ν_{24}	858(1/0.2)	832	849	856 w			870 vw		$C_3H/C_4H/C_5H/C_6H$ wag (oop)
ν_{25}	763(12/0.9)	740	756						$N_1H/C_3H/C_4H/C_5H/C_6H$ bend (oop)
ν_{26}	728(96/0.5)	706	721	709(w)					$N_1H(s)/C_3H/C_4H/C_5H/C_6H$ wag (oop)
ν_{27}	694(0.2/2)	673	688						ring torsion (oop)
ν_{28}	476(32/1)	462	475				491 vs		ring butterfly (oop)
ν_{29}	384(0/0.2)	372	385	389(w)			400 wsh		ring torsion (oop)
ν_{30}	143(0.6/0.1)	139	149						C_2S wag + ring oop

[a] B3LYP/6-311+G(d,p) calculated; values in parentheses are IR/Raman activities. [b] Scaled = $a \times 0.97$; oop: out-of-plane; bend: angular bend; s: strong; m: medium; w: weak; sh: shoulder; scanning = $a \times 0.97885 + 8.82622$; R.Raman: resonance Raman. [c] Ref 14.

state 2TP. The transient resonance Raman spectrum C in Figure 4, which is obtained by using ~260 μJ pulse energies focused on a beam diameter of ~0.5, is in intensity pattern and in vibrational frequency very different from the spectrum B. To identify the transient species that response to the spectrum C, (U)B3LYP/6-311+G(d,p) computations are carried out to determine the vibrational spectra of 2MP in S_0 and T_1 states and 2TP in T_1 state, and the results are listed in Table 3 and shown in Figure 5.

Figure 5 and Table 3 indicate that the ground state 2MP is likely the major species responsible for the transient Raman spectrum d since among sixteen A′ vibrational modes in the region 100−1700 cm^{-1}, and 11 observed bands can reasonably correlate to those of the ground state 2MP predicted by the B3LYP/6-311+G(d,p) computation. 2TP in T_1 state is unlikely the major species that is responsible for the transient resonance Raman spectrum of 2TP since the UB3LYP/6-311+G(d,p) predicted Raman frequencies are in general very different from those of the transient Raman spectrum. For example, the transient Raman spectrum displays two largest Raman bands at 973 and 735 cm^{-1}, but these two bands are not found in spectrum a of Figure 5 for 2TP in the T_1 state. Similarly, 2MP in the T_1 state is unlikely the major species that can globally meet the experimental transient resonance Raman spectrum of 2TP. Thus most of the transient resonance Raman features is assigned as about 11 totally symmetric fundamentals of 2MP.

We note that the generation of a transient Raman spectrum by the excitation of single laser line in the high pulse energy often leads to a complex mixture of different species. To unambiguously confirm the vibrational assignment of the transient resonance Raman spectrum C in Figure 4, we have also carried out the nanosecond time-resolved resonance Raman spectroscopic

dx.doi.org/10.1021/jp203185a |J. Phys. Chem. B 2011, 115, 8266–8277

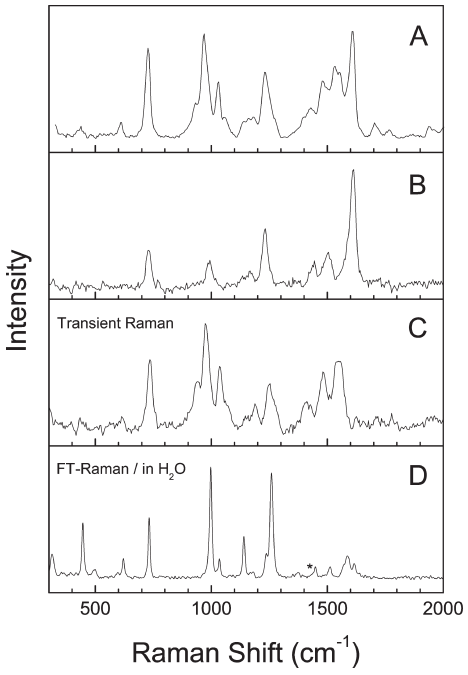

Figure 4. High power (A) and lower power (B) 266.0 nm resonance Raman spectra of 2-thiopyridone in water solution. Panel C is the difference spectrum between A and B. The FT-Raman spectrum in water solvent (D) is included for comparison.

measurement to study the time evolution behavior of the transient species. An examination of the nanosecond time-resolved resonance Raman spectra (266 nm pump and 266 nm probe) in Figure 6 indicates that the Raman bands attributable to the transient species have the strongest Raman intensity at 0 ns time delay. These resonance Raman bands decrease in intensity as time increases and vanish at about 110 ns simultaneously. This time evolution behavior indicates that these resonance Raman bands should mostly come from a single molecular species and thus confirms the assignment that the transient resonance Raman spectra C in Figure 4 is predominantly attributed to 2MP.

A further examination of Figure 6 reveals that the transient resonance Raman spectrum is different from those of the time-resolved resonance Raman spectra in several aspects. The line at 1485, 1253, 1188, and 940 cm^{-1} in the high pulse energy difference spectrum (Figures 4, 5, and 6) does not seem to be present in or dominate the time-resolved spectra of 2MP and the weak pulse energy resonance Raman spectrum of 2TP. This fact suggests that they may originate from the shorter-lived (subnanosecond) species such as 2TP in the T_1 state (Figure 5b) and/or 2MP in the T_1 state (Figure 5a). The laser power dependence of the Raman intensity of the parent 2TP relative to water solvent confirms the occurrence of the bulk photoalternation in higher laser power, and this indicates the high pulse energy difference spectrum is formed from a two-photon process. The line at 735 cm^{-1} for the transient resonance Raman spectrum is very close to the line at 731 cm^{-1} of the parent molecule, and its intensity is significantly more intense than those of the time-resolved spectra of the photoproduct. This difference is probably induced by the simple subtraction procedure (i.e., the constant multiplying one spectrum before subtraction from the other) that may cause the 731 cm^{-1} line to be under-subtracted since the photoproduct 2MP should have a different absorption spectrum from the parent 2TP, and the subtraction parameter that completely removes one 2TP line may not remove the others and thus makes the line intensity at 735 cm^{-1} become more intense.

Figure 7 displays the expanded view of the 266.0 nm resonance Raman spectra of 2TP in water solution. The vibrational assignments are listed in Table 2. The 266.0 nm resonance Raman spectrum of 2TP indicates that the excited state structural dynamics has significant multidimensional character with the largest contribution in the nominal $C_3{=}C_4/C_5{=}C_6$ stretch + ring deformation ν_6 since the fundamental (ν_6), its overtones, and their combination bands with the remaining seven vibrational modes occupy most of the Raman intensity. The moderate contributions come from the fundamentals and combination bands of the $N_1H/C_6H/C_3H$ bend ν_{12}, the $C_2{=}S$ stretch + ring deformation ν_{18}, and the $C_2{=}S$ stretch + ring deformation ν_{17}. The structural dynamics along the $C_3{=}C_4/C_5{=}C_6$ stretch and $C_2{=}S$ stretch reaction coordinates consists qualitatively with the electronic transition associated with the B-band absorption since $29{\rightarrow}31$ orbital transition weakens the bonds of $C_3{=}C_4$, $C_5{=}C_6$, and $C_2{=}S$. The structural dynamics along $N_1H/C_6H/C_3H$ bend reaction coordinates consists with the ESPT reaction since N_1H bend motion is dynamically required for proton to move from N atom to S atom, and this causes C_6H and C_3H bend reaction coordinates to become dynamically active.

The vibrational assignments of time-resolved resonance Raman spectra of 2MP are shown in Figure 6 and are listed in Table 3. The spectra display significantly the multidimensional structural dynamics. The largest intensity occurs at the ring deformation ν_{16} at 973 cm^{-1}, the $N_1{-}C_2/C_4{-}C_5$ stretch ν_7 at 1537 cm^{-1}, and the $N_1{-}C_6/C_3{-}C_4$ stretch ν_6 at 1557 cm^{-1}. The moderate Raman intensities happen to the ring breath ν_{18} at 733 cm^{-1} and the $C_4{-}C_5$-C_6 symmetric stretch ν_{15} at 1035 cm^{-1}, while minor Raman intensities occur at the $C_2{-}N_1{-}C_6/C_4{-}C_5{-}C_6$ antisymmetric stretch ν_{11} at 1253 cm^{-1}, the $C_3{-}H/C_6{-}H$ bend + $N_1{-}C_2$ stretch ν_8 at 1481 cm^{-1}, and the $N_1{-}C_6/C_2{-}C_3$ stretch + $C_4{-}H/C_5{-}H$ bend ν_9 at 1412 cm^{-1}. These eight fundamentals, their overtones, and combination bands occupy most of the remaining Raman intensities, and this suggests that they play a key role in the back proton transfer reaction of 2MP.

3.5. Discussion on the ESIPT Reaction Mechanism. The ESPT reaction of 2TP is detected by the present transient resonance Raman and nanosecond time-resolved resonance Raman spectroscopic observation of 2MP photoproduct. To explore the ESPT reaction mechanism, the global minimum structures, the vertical transition energies, and transition barriers between 2TP and 2MP for S_0, T_1, and/or S_1 states were obtained by using (U)B3LYP-TD/6-311+G(d,p) and CASPT2//CASSCF/6-311+G(d,p) level of theory computations, and the results are displayed in Figure 8 and Table 4. Figure 8 schematically depicts the potential energy surface diagram for the ESIPT processes. Figure 8 shows that the ground state 2MP is in energy higher than 2TP by 2.57 kcal/mol on the basis of the B3LYP/6-311++G(d,p) level of theory employing an SCRF and PCM. However the ground state proton transfer reaction between 2PT and 2MP is greatly prohibited due to the very high transition barrier of the proton transfer tautomerization reaction [30.2 kcal/mol on the basis of $2TP(S_0)$]. This is very similar to the ground state proton transfer reaction between 2HP and 2PY that has a transition barrier of 34−38 kcal/mol.[13,16,18] Apparently the transition barrier of the proton transfer tautomerization between 2TP and 2MP is ∼4−8 kcal/mol lower than that the corresponding value

Table 3. Resonance Raman Vibrational Bands and (U)B3LYP/6-311+G(d,p) Calculated Vibrational Frequencies for 2-Mercaptopyridine in S_0 and T_1 States and 2-Thiopyridone in the T_1 State

		calc.		expt.	
sym	mode	*a*	*b*	R. Raman	description
			2MP in S_0 State		
A′	ν_1	3200	3104		$C_3-H/C_4-H/C_5-H/C_6-H$ stretch
	ν_2	3190	3094		$C_3-H(s)$ /$C_4-H/C_5-H/C_6-H$ stretch
	ν_3	3173	3078		$C_3-H/C_4-H(s)/C_5-H/C_6-H$ stretch
	ν_4	3156	3061		$C_3-H/C_4-H/C_5-H/C_6-H(s)$ stretch
	ν_5	2685	2604		S−H stretch
	ν_6	1619	1570	1557	C_6-N_1/C_3-C_4 stretch
	ν_7	1601	1553	1537	C_2-N_1/C_4-C_5 stretch
	ν_8	1486	1441	1485	C_3-H/C_6-H bend + C_2-N_1 stretch
	ν_9	1449	1406	1412	N_1-C_6/C_2-C_3 stretch + C_4-H/C_5-H bend
	ν_{10}	1316	1277		C_3-H/C_6-H bend
	ν_{11}	1286	1247	1253	$C_2-N_1-C_6$ asym stretch/$C_3-C_4-C_5$ asym stretch
	ν_{12}	1176	1141		$C_3-H/C_4-H/C_5-H$ bend
	ν_{13}	1151	1116		C_2-S stretch + $C_4-H/C_5-H/C_6-H$ bend
	ν_{14}	1113	1080		C_3-H/C_5-H bend
	ν_{15}	1064	1032	1035	$C_4-C_5-C_6$ sym stretch
	ν_{16}	1001	971	976	ring deformation
	ν_{17}	897	870		S−H bend
	ν_{18}	737	715	735	ring breath
	ν_{19}	632	613		ring deformation
	ν_{20}	419	406		C_2-S stretch
	ν_{21}	278	270		C_4-S bend
A″	ν_{22}	1006	976		$C_3-H/C_4-H/C_5-H/C_6-H$ wag (oop)
	ν_{23}	979	950		$C_3-H/C_4-H/C_5-H/C_6-H$ wag (oop)
	ν_{24}	887	860		$C_3-H/C_6-H/C_5-H$ wag (oop)
	ν_{25}	768	745		$C_3-H/C_4-H/C_5-H/C_6-H$ wag (oop)
	ν_{26}	746	724		ring torsion (oop)
	ν_{27}	487	472		butterfly (oop)
	ν_{28}	410	398		ring torsion (oop)
	ν_{29}	257	249		S−H bend (oop)
	ν_{30}	168	163		butterfly (oop)
			2MP in T_1 State		
A	ν_1	3216	3120		C_3-H stretch
	ν_2	3196	3100		C_5-H stretch/C_6-H stretch
	ν_3	3283	3185		C_5-H stretch/C_6-H stretch/C_4-H stretch
	ν_4	3157	3062		C_4-H stretch/C_5-H stretch
	ν_5	2660	2580		S−H stretch
	ν_6	1538	1492	1485	$C_4=C_5$ stretch
	ν_7	1458	1414		$N_1=C_2$ stretch
	ν_8	1390	1348		N_1-C_6 stretch/C_3-C_4 stretch
	ν_9	1371	1330		$C_2-C_3-C_4$ asym stretch/$C_5-C_6-N_1$ asym stretch
	ν_{10}	1313	1274	1253	$N_1=C_2$ stretch/C_3-H bend/C_6-H bend
	ν_{11}	1197	1161	1188	C_3-H bend/C_4-H bend/C_5-H bend/C_6-H bend
	ν_{12}	1110	1077		C_2-S stretch/C_3-H bend/C_5-H bend
	ν_{13}	1073	1041		ring deformation
	ν_{14}	965	936	940	C_4-H wag/C_5-H wag
	ν_{15}	960	931		S−H bend/ring deformation
	ν_{16}	913	886		S−H bend/ring breath
	ν_{17}	831	806		C_2-S stretch/S−H bend
	ν_{18}	715	694		C2−S stretch/ring deformation
	ν_{19}	699	678		C_4-H wag/C_5-H wag/C_6-H wag

dx.doi.org/10.1021/jp203185a |*J. Phys. Chem. B* 2011, 115, 8266–8277

Table 3. Continued

sym	mode	calc.		expt.	description
		a	*b*	R. Raman	
	ν_{20}	606	588		ring deformation
	ν_{21}	584	566		ring torsion
	ν_{22}	538	522		$C_2-N_1-C_6$ asym stretch/$C_3-C_4-C_5$ asym stretch
	ν_{23}	510	495		C_3-H wag/C_5-H wag/C_6-H wag
	ν_{24}	402	390		$S-H$ wag/C_3-H wag/C_4-H wag/C_6-H wag
	ν_{25}	386	374		$S-H$ wag/ring deformation
	ν_{26}	352	341		$S-H$ wag/C_3-H wag/C_4-H wag/C_6-H wag
	ν_{27}	335	325		$S-H$ wag/C_3-H wag/C_4-H wag/C_6-H wag
	ν_{28}	267	259		$C-S$ bend
	ν_{29}	248	241		$C-S$ wag/ring torsion
	ν_{30}	51	49		C_4-H stretch/C_5-H stretch
			2TP in T_1 State		
A	ν_1	3656	3546		N_1-H stretch
	ν_2	3235	3138		C_5-H stretch/C_6-H stretch/C_4-H stretch
	ν_3	3225	3128		C_3-H stretch/C_6-H stretch/C_4-H stretch
	ν_4	3211	3115		C_4-H stretch/C_3-H stretch
	ν_5	3184	3088		C_5-H stretch/C_6-H stretch/C_4-H stretch
	ν_6	1568	1521		$C_2=C_3-C_4$ asym stretch
	ν_7	1532	1486	1485	$C_5=C_6-N_1$ asym stretch
	ν_8	1446	1403		C_5-C_4 stretch
	ν_9	1438	1395		N_1-H bend/$C_3=C_2-N_1$ asym stretch
	ν_{10}	1378	1337		N_1-C_6 stretch/C_5-C_4 stretch
	ν_{11}	1278	1240	1253	N_1-H bend/C_6-H bend/C_5-H bend
	ν_{12}	1216	1180	1188	C_2-S stretch/C_5-C_4 stretch
	ν_{13}	1080	1048		C_2-S stretch/ring deformation
	ν_{14}	1076	1044		C_2-S stretch/$C_3-C_4-C_5$ asym stretch
	ν_{15}	1008	978		ring deformation
	ν_{16}	989	959	940	$N_1-C_2-C_6$ sym stretch/ring breath
	ν_{17}	953	924		C_4-H wag/C_5-H wag/C_6-H wag
	ν_{18}	937	909		ring breath
	ν_{19}	847	822		C_3-H wag (oop)
	ν_{20}	724	702		ring deformation
	ν_{21}	656	636		C_3-H wag/C_4-H wag/C_6-H wag
	ν_{22}	625	606		C_4-H wag/C_5-H wag/C_6-H wag
	ν_{23}	605	587		ring torsion
	ν_{24}	588	570		ring deformation
	ν_{25}	474	460		ring torsion (oop)
	ν_{26}	431	418		ring breath
	ν_{27}	296	287		ring bend
	ν_{28}	290	281		N_1-H wag
	ν_{29}	233	226		ring torsion (oop)
	ν_{30}	109	106		ring butterfly (oop)

[a] B3LYP/6-311+G(d,p). [b] Scaled = $a \times 0.97$ oop: out-of-plane; bend: angular bend; s: strong.

between 2HP and 2PY in water solution. Similarly 2MP(T_1, min) is in energy higher than 2TP(T_1, min) by 32.8 kcal/mol, and the transition barrier is 46.7 kcal/mol on the basis of 2TP(T_1, min). This indicates that the proton transfer tautomerization between 2TP(T_1) and 2MP(T_1) is also greatly hindered.

A further examination of Table 1 and Figure 2 suggests that the S_4 state of 2TP and the S_3 state of 2MP are two correlated singlet excited states that are possibly responsible for the excited state intramolecular proton transfer (ESIPT) reaction of 2TP. Since the vertical transition energy of the S_3 state of 2MP is 122 kcal/mol, which is much higher than 104 kcal/mol that is the vertical transition energy of the S_4 state of 2TP, direct formation of the S_3 state of 2MP through ESIPT reaction of 2TP is unlikely upon 266.0 nm excitation. Therefore, the role of the S_3 state of 2MP in the formation of the ground state 2MP is ruled out. Similarly the S_2 state of 2MP is expected to play minor role in the ESIPT reaction of 2TP since their vertical transition energies are significantly higher than that of the S_4 state of 2TP, and the

dx.doi.org/10.1021/jp203185a |J. Phys. Chem. B 2011, 115, 8266–8277

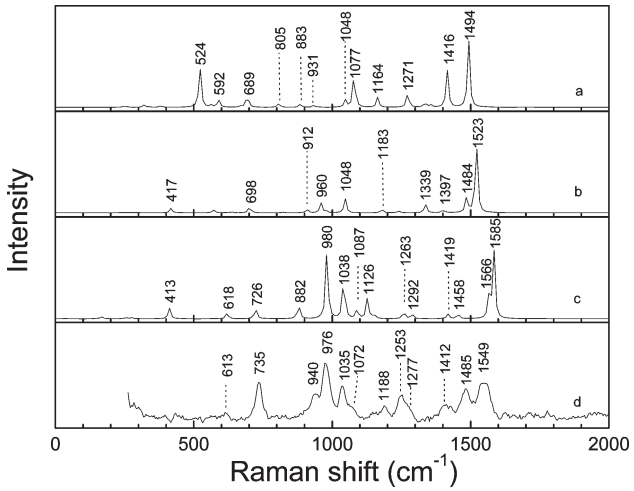

Figure 5. Comparison of the experimental transient resonance Raman spectrum (d) of 2-thiopyridone with the (U)B3LYP/6-311+G(d,p) computed Raman spectra for the ground state 2-mercaptopyridine (c), the lowest triplet 2-thiopyridone (b), and the lowest triplet 2-mercaptopyridine (a). The calculated frequencies in *x* axis of spectra a, b, and c are all scaled by a factor of 0.97.

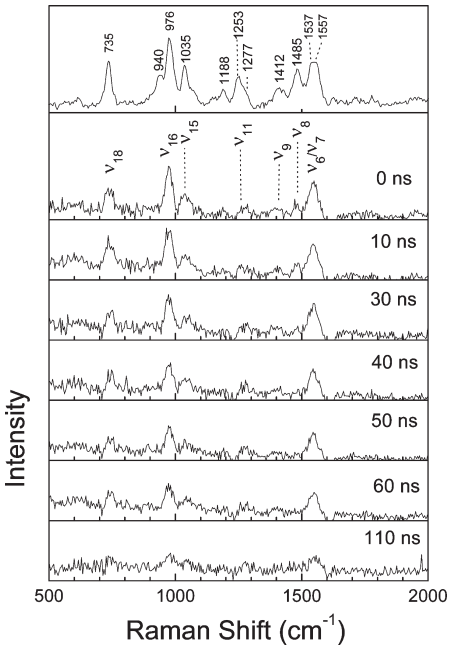

Figure 6. Nanosecond time-resolved resonance Raman spectra of 2MP photoproduct produced from ultraviolet excitation of 2TP in water solvent. Spectra were obtained at varing pump (266 nm) and probe (266 nm) time delays, which are indicated above each spectrum. The tentative vibrational assignments are indicated above the 0 ns spectrum.

available energy provided by 266 nm excitation (108 kcal/mol) is unlikely large enough to reach the S_2 state of 2MP.

The S_2 state of 2TP and the S_1 state of 2MP are two correlated $^1(\pi\pi^*)$ singlet excited states that are responsible for ESIPT tautomerization reaction between 2TP and 2MP. The very similar transition barriers for the ground state proton transfer tautomerization reactions between 2TP and 2MP and between 2HP and 2PY lead us to believe that the transition barrier of the

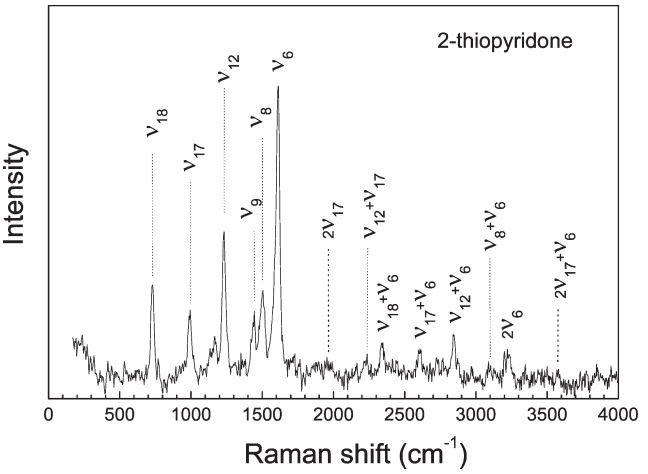

Figure 7. Expanded view of the 266.0 nm resonance Raman spectra of 2-thiopyridone with the tentative vibrational assignments indicated above the spectrum.

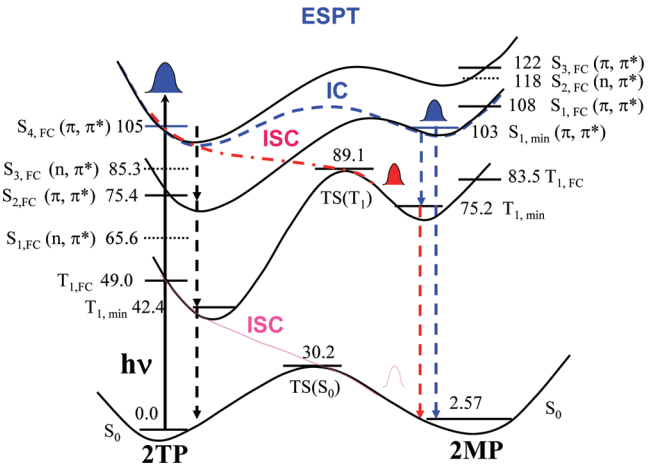

Figure 8. Potential energy surfaces diagram for ESPT tautomerization reactions between 2TP and 2MP. Vertical transition energies are estimated by (U)B3LYP-TD/6-311+G(d,p) level of theory for T_1, S_1, S_2, S_3, and S_4 states of 2-thiopyridone and T_1, S_1, S_2, and S_3 states of 2-mercaptopyridine. the minimum energy for S_1 state of 2-mercaptopyridine is calculated by the CASSCF(6,8)/6-311+G(d,p) level of theory. Values are in kcal/mol.

tautomerization reaction between the S_1 state of 2MP and the S_2 state of 2TP in water solution will be less than the transition barrier (5.6 kcal/mol) of the S_1 tautomerization between the 2HP and 2PY in water solution.[13] Since the vertical transition energy for the S_2 state of 2TP is 75.4 kcal/mol, which is much lower than that (108 kcal/mol) of the S_1 state of 2MP, the ESPT reaction from the S_2 state of 2TP to the S_1 state of 2MP is greatly prohibited.

Three possible decay reaction channels are suggested for the formation of 2MP, as shown in Figure 8. The ESPT reaction between the S_4 state of 2TP and the S_1 state of 2MP is in energy possible since the minimum energy of the $S_{1,min}$ state of 2MP predicted by CASPT2 level of theory calculation is 103 kcal/mol, which is very close to the vertical transition energy (105 kcal/mol) of the S_4 state of 2TP. The transition barriers between the S_4 state of 2TP and the S_1 state of 2MP are not presently determined due to the difficulty in CASSCF calculations. However this barrier is

Table 4. B3LYP/6-311+G(d,p) Computed Bond Lengths (Å) and Bond Angles (deg) for Various S_0, T_1, and/or S_1 State Proton-Transfer Tautomers of 2-Thiopyridone and Their Corresponding Transition States and CASSCF/6-311+G(d,p) Computed Bond Lengths (Å) and Bond Angles (deg) for S_1 of 2MP

	S_0			T_1			S_1
parameter	S_0(2TP)	S_0(2MP)	TS(S_0)(2TP-2MP)	$T_{1,min}$(2TP)	$T_{1,min}$(2MP)	TS($T_{1,min}$)(2TP-2MP)	$S_{1,min}$(2MP)
R_{N1-C2}	1.38	1.33	1.36	1.41	1.31	1.46	1.37
R_{C2-C3}	1.43	1.40	1.40	1.37	1.51	1.39	1.43
R_{C3-C4}	1.37	1.39	1.39	1.44	1.41	1.39	1.43
R_{C4-C5}	1.42	1.40	1.40	1.39	1.36	1.45	1.42
R_{N1-C6}	1.36	1.34	1.34	1.39	1.34	1.34	1.36
R_{C2-S7}	1.68	1.79	1.73	1.72	1.74	1.71	1.75
R_{C3-H8}	1.08	1.08	1.08	1.08	1.08	1.08	1.07
R_{C4-H9}	1.08	1.08	1.08	1.08	1.08	1.08	1.07
R_{C5-H10}	1.08	1.08	1.08	1.08	1.08	1.08	1.07
R_{C6-H11}	1.08	1.08	1.08	1.08	1.08	1.08	1.07
R_{N1-H12}(2TP)	1.01		1.36	1.00		1.46	
R_{S7-H12}(2MP)		1.35			1.35		1.33
$\angle_{N1-C2-C3}$	114	123	120	119	124	123	125
$\angle_{C2-C3-C4}$	122	118	118	121	116	119	119
$\angle_{C3-C4-C5}$	121	119	121	117	120	117	116
$\angle_{C2-N1-C6}$	126	118	122	122	119	116	115
$\angle_{N1-C2-S7}$	120	118	105	117	121	101	117
$\angle_{C2-C3-H8}$	117	121	120	118	121	118	119
$\angle_{C3-C4-H9}$	120	120	119	121	120	121	122
$\angle_{C4-C5-H10}$	122	122	121	120	121	120	121
$\angle_{N1-C6-H11}$	116	116	116	124	118	117	116
$\angle_{C6-N1-H12}$(2TP)	120		154	121		114	
$\angle_{C2-S7-H12}$(2MP)		94			95		96
$D_{N1-C2-C3-C4}$	0	0	0	−0.01	0.05	−1.33	0.07
$D_{C2-C3-C4-C5}$	0	0	0	−0.04	−0.04	−3.72	−0.06
$D_{C3-C2-N1-C6}$	0	0	0	0.03	−0.01	6.74	−0.07
$D_{C6-N1-C2-S7}$	180	180	180	−179.9	179.9	−166	−179.0
$D_{N1-C2-C3-H8}$	180	180	180	179.9	179.9	179	−179.5
$D_{C2-C3-C4-H9}$	180	180	180	179.9	179.9	179	−179.6
$D_{C3-C4-C5-H10}$	180	180	180	−179.9	179.9	−176	−179.6
$D_{C2-N1-C6-H11}$	180	180	180	−179.9	179.9	175	179.8
$D_{C5-C6-N1-H12}$(2TP)	180		180	−179.8		−145	
$D_{N1-C2-S7-H12}$(2MP)		0			−0.005		−1.43

expected to be small since the corresponding orbitals are similar for two $\pi \rightarrow \pi^*$ transitions of 2TP and 2MP. Thus 2TP in S_4 state would have enough available energy to overcome the transition barrier and finally tautomerize to the $S_{1,min}$ state of 2MP upon 266 nm excitation, and this is referred to as the IC channel (blue dash curve in Figure 8). The second possible way of 2MP formation is the ISC channel (red dot−dash curve in Figure 8), in which the S_4 state of 2TP decays to the T_1 state of 2MP with the aid of intersystem crossing mechanism and through the global T_1 potential energy surface connecting both 2MP and 2TP since the transition state TS($T_{1,min}$)(2TP-2MP) is in energy below that of the S_4 state of 2TP. The third possible channel is from the T_1 state of 2TP to the ground state 2MP (magenta dotted curve in Figure 8) since the T_1 state of 2TP could be formed in several ways.

It is interesting to note that the geometry structures of S_0(2MP), $T_{1,min}$(2MP), and $S_{1,min}$(2MP) are very similar to one another, although some bond lengths are somewhat different as shown in Table 4. This provides two further decay channels for $S_{1,min}$(2MP) to follow if it were formed. One is the direct vibrational relaxation from $S_{1,min}$(2MP) to the ground state 2MP. The other is the ISC to $T_{1,min}$(2MP) and then to the ground state 2MP. The very high transition barrier between $T_{1,min}$(2MP) and $T_{1,min}$(2TP) makes the trapped transient species $T_{1,min}$(2MP) be hardly back to $T_{1,min}$(2TP) once the S_4 state of 2TP passes over the transition state TS($T_{1,min}$)(2TP-2MP). Therefore, the S_1 and T_1 states of 2MP and T_1 states of 2TP are three most likely intermediate states that lead to the final formation of the ground state 2MP.

Further experimental and theoretical works are required to unambiguously clarify whether the proposed ESPT reaction mechanism of 2TP that leads to the final formation of 2MP is correct or not. Advanced CASSCF calculations using different solvent models and PCM/TD-PBE0 (the time-dependent density-functional theory level, using the polarizable continuum model)[53] considering different water complexes are very helpful in accurately

predict the excited state potential energy surfaces and the curve crossings between different excited state species. According to Figure 8, the determination of the internal conversions or intersystem crossing between the S_4 state of 2TP and the S_2 and S_1 or T_1 states of 2MP, as well as intersystem crossing between T_1 and S_0 of 2MP, is especially important to make clear the reaction mechanism for the ground state 2MP formation. Ultrafast (fs and ps) to nanosecond (ns) time-resolved spectroscopic experiments that confirm the existence of 2MP(T_1) and/or 2TP(T_1) species are firmly required to tackle the issue for whether the ground state 2MP is formed directly from $S_{1,min}$(2MP) or from the intermediate state $T_{1,min}$(2MP) and/or $T_{1,min}$(2TP).

4. CONCLUSION

The photomeric tautomerization reaction between 2TP and 2MP is studied by using both the resonance Raman and nanosecond time-resolved resonance Raman spectroscopy. The resonance Raman spectra were obtained for both 2-thiopyridone (2TP) and its proton-transfer tautomer 2-mercaptopyridine (2MP) in water solution. The ultraviolet electronic transitions and the 266.0 nm resonance Raman spectra of 2TP and 2MP are assigned with the help of the DFT calculations. The time evolution behavior of the transient species, revealed by the nanosecond time-resolved resonance Raman experiment, confirms the assignment that the transient resonance Raman spectra C in Figure 4 is attributed to 2MP. The different short-time structural dynamics were examined for both 2TP and 2MP in terms of the resonance Raman intensity patterns, and the results indicate that most of the 266.0 nm resonance Raman features of 2TP can be assigned as about eight totally symmetric fundamentals and the excited state structural dynamics has significant multidimensional character with the largest contribution in the nominal $C_3{=}C_4/C_5{=}C_6$ stretch + ring deformation ν_6 at 1614 cm^{-1}, while most of the 266.0 nm resonance Raman spectrum of 2MP can be assigned as about 11 totally symmetric fundamentals, and the excited state structural dynamics also displays that the significant multidimensional character with the largest intensity occurs at the ring deformation ν_{16} at 973 cm^{-1}. The transition barriers between 2TP and 2MP for S_0, T_1, and S_1 states are determined by using (U)B3LYP-TD and CASSCF level of theories, respectively. The ESPT reaction mechanism is proposed with the aid of CASSCF and TD-DFT computations made for both 2MP and 2TP. Our results indicate that the ESPT reaction of 2TP in water solution leads to the formation of the 2MP transient species, which constitutes an important excited state decay channel for 2TP upon 266 nm excitation.

AUTHOR INFORMATION

Corresponding Author

*Fax: 86-0571-86843699. E-mail: zxm@zstu.edu.cn.

ACKNOWLEDGMENT

This work was supported by grants from the National Natural Science Foundation of China (NSFC, Nos. 21033002 and 20573097) and the National Basic Research Program of China (2007CB815203).

REFERENCES

(1) Nimlos, M. R.; Kelley, D. F.; Bernstein, E. R. *J. Phys. Chem.* **1989**, *63*, 643–651, and references therein.
(2) Held, A.; Pratt, D. W. *J. Am. Chem. Soc.* **1993**, *115*, 9708–9717.
(3) Matuda, Y. T.; Ebata, Mikami, N. *J. Chem. Phys.* **1999**, *110*, 8397–8407.
(4) Matuda, Y.; Ebata, T.; Mikami, N. *J. Chem. Phys.* **2000**, *113*, 573–580.
(5) Matuda, Y.; Ebata, T.; Mikami, N. *J. Phys. Chem. A* **2001**, *105*, 3475–3480.
(6) Nowak, M. L.; Lapinski, L.; Fulara, J.; Les, A. L.; Adamowicz *J. Phys. Chem.* **1992**, *96*, 1562–1569.
(7) Beak, P. *Acc. Chem. Res.* **1977**, *10*, 186–192.
(8) Hatherley, L. D.; Brown, R. D.; Godfrey, P. D.; Pierlot, A. P.; Caminati, W.; Damiani, D.; Melandri, S.; Favero, L. B. *J. Phys. Chem.* **1993**, *97*, 46–51.
(9) Sanchez, R.; Giuliano, B. M.; Melandri, S.; Favero, L. B.; Caminati, W. *J. Am. Chem. Soc.* **2007**, *129*, 6287–6290.
(10) Fujimoto, A.; Inuzuka, K.; Shiba, R. *Bull. Chem. Soc. Jpn.* **1981**, *54*, 2802–2806.
(11) Sakota, K.; Tokuhara, S.; Sekiya, H. *Chem. Phys. Lett.* **2007**, *448*, 159–163.
(12) Florio, G. M.; Gruenloh, C. J.; Quimpo, R. C.; Zwier, T. S. *J. Chem. Phys.* **2000**, *113*, 11143–11153.
(13) Moreno, M.; Miller, W. H. *Chem. Phys. Lett.* **1990**, *171*, 475–479.
(14) Sobolewski, A. L. *Chem. Phys. Lett.* **1993**, *211*, 293–299.
(15) Barone, V.; Adamo, C. *Chem. Phys. Lett.* **1994**, *226*, 399–404.
(16) Barone, V.; Adamo, C. *J. Phys. Chem.* **1995**, *99*, 15062–15068.
(17) Sobolewski, A. L.; Adamowicz, L. *J. Phys. Chem.* **1996**, *100*, 3933–3941.
(18) Li, Q. S.; Fang, W. H.; Yu, J. G. *J. Phys. Chem. A* **2005**, *109*, 3983–3990.
(19) Wang, J.; Boyd, R. J. *J. Phys. Chem.* **1996**, *100*, 16141–16146.
(20) Del Bene, J. E. *J. Am. Chem. Soc.* **1995**, *117*, 1607–1610.
(21) Chou, P. T.; Wei, C. Y.; Hung, F. T. *J. Phys. Chem. B* **1997**, *101*, 9119–9126.
(22) Dkhissi, A.; Adamowicz, L.; Maes, G. *J. Phys. Chem. A* **2000**, *104*, 5625–5630.
(23) Esboui, M.; Nsangou, M.; Jaidane, N.; Ben Lakhdar, Z. *Chem. Phys.* **2005**, *311*, 277–285.
(24) Krebs, C.; Forster, W.; Weiss, C.; Hofmann, H. J. *J. Prakt. Chem.* **1982**, *324*, 369–378.
(25) Esboui, M.; Jaidane, N.; Ben Lakhdar, Z. *Chem. Phys. Lett.* **2006**, *430*, 195–203.
(26) Lowdin, P. O. *Rev. Mol. Phys.* **1963**, *35*, 724.
(27) Pullman, B.; Pullman, A. *Adv. Heterocycl. Chem.* **1971**, *13*, 77–159.
(28) Beak, P.; Covington, J. B.; Smith, S. G. *J. Am. Chem. Soc.* **1976**, *98*, 8284–8286.
(29) Beak, P.; Fry, F. S., Jr.; Lee, J.; Steele, F. *J. Am. Chem. Soc.* **1976**, *98*, 171–184.
(30) Melandri, S.; Evangelisti, L.; Maris, A.; Caminati, W.; Giuliano, B. M.; Feyer, V.; Prince, K. C.; Coreno, M. *J. Am. Chem. Soc.* **2010**, *132*, 10269–10271.
(31) Jones, P. A.; Katritzky, A. R. *J. Chem. Soc.* **1958**, 3610–3613.
(32) Katritzky, A. R.; Jones, R. A. *J. Chem. Soc.* **1960**, 2947–2953.
(33) Cook, M. J.; Katritzky, A. R.; Linda, P.; Tack, R. D. *J. Chem. Soc., Perkin Trans.* **1972**, *2*, 1295–1301.
(34) Albert, A.; Barlin, G. B. *J. Chem. Soc.* **1959**, 2384–2396.
(35) Stoyanov, S.; Petkov, I.; Antonov, L.; Stoyanova, T.; Karagiannidis, P.; Aslanidis, P. *Can. J. Chem.* **1990**, *68*, 1482–1489.
(36) Barlin, G. B.; Brown, D. J.; Fenn, M. D. *Aust. J. Chem.* **1984**, *37*, 2391–2395.
(37) Spinner, E. *J. Chem. Soc.* **1960**, 1237–1242.
(38) Lapinski, L.; Nowak, M. J.; Fulara, J.; Les, A.; Adamowicz, L. *J. Phys. Chem.* **1992**, *96*, 6250–6254.
(39) Contreras, J. G.; Alderete, J. B. *J. Mol. Struct.: THEOCHEM* **1991**, *231*, 257–265.
(40) Pang, Y. S.; Hwang, H. J.; Kim, M. S. *J. Mol. Struct.* **1998**, *441*, 63–76.

(41) Colthup, N. B.; Daly, L. H.; Wiberley, S. E. *Introduction to Infrared and Raman Spectroscopy*, 3rd ed.; Academic Press: New York, 1990.
(42) Santhayanarayana, D. N. *Vibrational Spectroscopy, Theory and Applications*, Vol. 4; New Age International Publishers: New Delhi, 2004.
(43) Krishnakumar, V.; Xavier, R. J. *Spectrochim. Acta, Part A* **2006**, *63*, 454–463.
(44) Abdulla, H. I.; El-Bermani, M. F. *Spectrochim. Acta, Part A* **2001**, *57*, 2659–2671.
(45) Kwok, W. M.; Phillips, D. L. *J. Chem. Phys.* **1996**, *104*, 2529–2540.
(46) Zheng, X.; Phillips, D. L. *J. Chem. Phys.* **1998**, *108*, 5772–5783.
(47) Zheng, X.; Li, Y. L.; Phillips, D. L. *J. Phys. Chem. A* **2004**, *108*, 8032–8039.
(48) Zhu, X. M.; Zhang, S. Q.; Zheng, X.; Phillips, D. L. *J. Phys. Chem. A* **2005**, *109*, 3086–3093.
(49) Weng, K. F.; Shi, Y.; Zheng, X.; Phillips, D. L. *J. Phys. Chem. A* **2006**, *110*, 851–860.
(50) Li, Y. L.; Leung, K. H.; Phillips, D. L. *J. Phys. Chem. A* **2001**, *105*, 10621–10625.
(51) Frisch, M. J.; Trucks, G. W.; Schlegel, H. B.; Scuseria, G. E.; Robb, M. A.; Cheeseman, J. R.; Montgomery, J. A., Jr.; Vreven, T.; Kudin, K. N.; Burant, J. C.; Millam, J. M.; Iyengar, S. S.; Tomasi, J.; Barone, V.; Mennucci, B.; Cossi, M.; Scalmani, G.; Rega, N.; Petersson, G. A.; Nakatsuji, H.; Hada, M.; Ehara, M.; Toyota, K.; Fukuda, R.; Hasegawa, J.; Ishida, M.; Nakajima, T.; Honda, Y.; Kitao, O.; Nakai, H.; Klene, M.; Li, X.; Knox, J. E.; Hratchian, H. P.; Cross, J. B.; Adamo, C.; Jaramillo, J.; Gomperts, R.; Stratmann, R. E.; Yazyev, O.; Austin, A. J.; Cammi, R.; Pomelli, C.; Ochterski, J. W.; Ayala, P. Y.; Morokuma, K.; Voth, G. A.; Salvador, P.; Dannenberg, J. J.; Zakrzewski, V. G.; Dapprich, S.; Daniels, A. D.; Strain, M. C.; Farkas, O.; Malick, D. K.; Rabuck, A. D.; Raghavachari, K.; Foresman, J. B.; Ortiz, J. V.; Cui, Q.; Baboul, A. G.; Clifford, S.; Cioslowski, J.; Stefanov, B. B.; Liu, G.; Liashenko, A.; Piskorz, P.; Komaromi, I.; Martin, R. L.; Fox, D. J.; Keith, T.; Al-Laham, M. A.; Peng, C. Y.; Nanayakkara, A.; Challacombe, M.; Gill, P. M. W.; Johnson, B.; Chen, W.; Wong, M. W.; Gonzalez, C.; Pople, J. A. *Gaussian 03, Revision B.05*; Gaussian, Inc.: Pittsburgh, PA, 2003.
(52) Marian, C. M. *J. Chem. Phys.* **2005**, *122*, 104314–104326.
(53) Santoro, F.; Barone, V.; Gustavsson, T.; Improta, R. *J. Am. Chem. Soc.* **2006**, *128*, 16312–16322.